Technical Notes

Second Mode Suppression in Hypersonic Boundary Layer by Roughness: Design and Experiments

Kahei Danny Fong,* Xiaowen Wang,† Yuet Huang,* and Xiaolin Zhong‡
University of California, Los Angeles, California 90095
and
Gregory R. McKiernan,§ Roy A. Fisher,¶ and Steven P. Schneider**
Purdue University, West Lafayette, Indiana 47907-1282

DOI: 10.2514/1.J054100

I. Introduction

THE performance of hypersonic transportation vehicles and reentry vehicles is significantly affected by the laminar-turbulent transition of boundary-layer flows over vehicle surfaces, as transition has a first-order impact on the lift, drag, stability, control, and surface heating. For a reentry vehicle, transition can lead to an increase in the surface heating rate by a factor of five or more. Hence, the understanding of transition mechanisms and the prediction of transition locations are critical to the development of future hypersonic vehicles [1].

One important area of transition study is the effect of roughness on hypersonic boundary-layer transition. Despite several decades of experimental, theoretical, and numerical studies, the effect of surface roughness on transition is still not fully understood [2]. Most previous research has focused mainly on tripping the flow using roughness elements. However, there have been a few reported experimental and numerical studies that demonstrate a delay of transition by roughness elements under certain circumstances. James [3] experimentally studied the effects of Mach number and surface roughness on boundary-layer transition using fin-stabilized hollow tube models in free flights. James found that, for some Mach numbers, there exists an optimum roughness height that results in a longer laminar run on a rough surface than a smooth surface. In other words, the roughness element delays the transition process rather than promoting it. Holloway and Sterrett [4] performed a transition experiment in the Langley 20 in. Mach 6 tunnel using a flat plate embedded with spherical roughness elements. They found that, for the cases with the smallest roughness diameters, transition was delayed under certain flow conditions. Although they did not investigate the reasons or conditions behind the delay, they hypothesized that the roughness creates a separated laminar mixing layer that is more stable at higher Mach numbers. More recently, Fujii [5] performed experiments using a 5 deg half-angle sharp cone at Mach 7. The tests were completed at stagnation pressures of 2, 4, and 6 MPa. It was found that, for the higher-pressure cases, the onset of transition was delayed when the wavelength of the wavy wall roughness was roughly equal to that of the unstable second-mode wavelength. Although the delay effect is weak, it is still discernible, and the repeatability of the results is remarkably good. It was speculated that there is a relationship between the wavy wall wavelength and second-mode disturbance that leads to transition. However, the mechanism of the transition delay was unknown and not explored.

In addition to experimental testing, several numerical studies have reported the roughness effects on transition delay. Marxen et al. [6] studied the disturbance growth on a flat-plate boundary layer at Mach 4.8 with localized two-dimensional (2-D) roughness elements. They found the disturbance was strongly damped downstream of the roughness element around the separation region, which agrees with Holloway and Sterrett's [4] hypothesis. However, the mechanisms were not investigated. At the same time, Duan et al. [7] from University of California, Los Angeles (UCLA) reported that a 2-D roughness element can damp disturbances if the element is placed downstream of the location where the slow hypersonic boundary-layer mode (mode *S*) and fast hypersonic boundary-layer mode (mode *F*) have the same phase velocity (the synchronization location). The details of the work by the UCLA group will be discussed in the next paragraph. Riley et al. [8,9] also numerically studied the stability characteristics of a Mach 4 hypersonic boundary layer over a wedge. On the surface of the wedge, they imposed convex or concave panel buckling (compliant panel) at different locations. They found that, when the panel is placed near the trailing edge of the wedge, the panel can move the boundary-layer transition further downstream. On the other hand, Egorov et al. [10] performed numerical simulations of a Mach 6 supersonic boundary layer over a grooved wavy plate. Their study was motivated by the numerical studies of Balakumar [11] and Egorov et al. [12], which showed the second mode remains neutral in the separated region on a 5.5 deg compression corner. Based on the result of the separated region, the intention of the study by Egorov et al. was to generate short local boundary-layer separations by the wavy wall to decrease disturbance growth. The wavy wall was in the form of nine round arc cavities. It was found that the wavy wall design damps a range of high-frequency unstable disturbances that are relevant to the second-mode instability. Bountin et al. [13] later confirmed the results by Egorov et al. [10] that the wavy wall damps the unstable second mode in the high-frequency band while it enhances them at lower frequencies. Their experimental data [13] also showed that the wavy wall damps disturbances, not only at the wavy wall wavelength but also at a wide range of disturbances in different frequencies with different wavelengths. Based on these results, they argued that the stabilization effect of the second mode by the wavy wall is due to altering the mean flow instead of an interference process between the second mode and the wavy wall itself.

Since 2009, for the purpose of simulating hypersonic flow with finite height roughness elements, Duan et al. has developed a high-order cut-cell method [14]. The new method was then applied to simulating finite roughness elements in a hypersonic boundary layer at Mach 5.92 [7,14]. Different from the wavy wall idea, as in [5] and [10], they found that the relative location of the 2-D roughness

Received 4 December 2014; revision received 7 April 2015; accepted for publication 8 April 2015; published online 8 June 2015.

*Graduate Research Assistant, Mechanical and Aerospace Engineering Department. Student Member AIAA.

†Research Associate, Mechanical and Aerospace Engineering Department. Senior Member AIAA.

‡Professor, Mechanical and Aerospace Engineering Department. Associate Fellow AIAA.

§Graduate Research Assistant, School of Aeronautics and Astronautics. Student Member AIAA.

¶Graduate Student, School of Aeronautics and Astronautics.

**Professor, School of Aeronautics and Astronautics. Associate Fellow AIAA.

element and the synchronization location plays an important role [7]. The synchronization location is the point where the mode *S* and mode *F* disturbance have the same phase velocity. More detail about the synchronization location can be found in [15,16]. Zhong's group argues that 2-D roughness elements can damp 2-D disturbances if the roughness element, with a height less than the local boundary-layer thickness, is downstream of the synchronization point [14]. This finding has motivated a series of parametric studies on roughness effects including roughness locations, heights, and widths by Fong et al. [17–19]. All results are consistent with the initial finding that 2-D roughness elements can damp 2-D disturbances and have shown the importance of roughness locations and synchronization locations. In 2013, Park and Park [20] performed a theoretical parabolized stability equations (PSE) study of a smooth hump on a hypersonic flat plate to investigate the importance of the synchronization location as Fong et al. discovered [21]. They found the stabilization effect of the hump on convective instability is possible and confirmed the idea of the importance of the roughness location and the synchronization point.

Based on the direct numerical simulation (DNS) results, which show the importance of the roughness location and synchronization point, the onset of hypersonic boundary-layer transition can be delayed by judiciously placed 2-D roughness elements downstream of the synchronization location for the most dangerous disturbance determined by a linear stability analysis. In this Note, the flow control design is presented for a specific case on a compression flared cone at Mach 6, followed by the corresponding experimental results.

II. Steady Base Flow and Stability Properties

A. Test Model and Flow Conditions

A hypersonic flow over an axisymmetric flared cone is used for the current study. The compression cone geometry is based on the experiment of Wheaton et al. [22]. It is a blunt cone with a 1-mm-radius spherical nose and a concave flaring right behind the nose, which is designed such that the boundary-layer thickness along the cone remains constant in the current flow condition. The initial half angle is 2 deg. The flaring is a circular arc of 3 m in radius. The cone has a total length of approximately 0.45 m.

The freestream conditions used in the numerical simulations in this study are based on The Boeing Company/U.S. Air Force Office of Scientific Research Mach 6 Quiet Tunnel [22], for which the freestream unit Reynolds number is 1.026×10^7 m^{-1} and the Mach number is 6. Huang and Zhong [23] had more details on the freestream conditions. Since the cone is at zero angle of attack, it is assumed that the flow around the cone is axisymmetric. The surface of the cone is assumed to be rigid, smooth, and isothermal in this study. This case is chosen because it is a benchmark that has been studied without roughness [24]. In the study of the smooth compression cone at the current freestream condition by Wheaton et al. [22], no transition was observed, and the maximum *N* factor obtained from linear stability equation (LST) reached 14 at the end of the cone. In addition, Huang and Zhong [23,25–28] have conducted extensive numerical and stability studies of boundary-layer receptivity to freestream hotspot perturbations with the same freestream conditions over a compression cone.

B. Steady Base Flow and Linear Stability Properties

The steady base flow and linear stability properties were computed by Huang and Zhong [23]. They are presented briefly in this Note. The pressure contours of the steady base flow are shown in Fig. 1a. Pressure is initially very large in the nose region, and it decreases rapidly downstream of the nose region. In the long flaring, or compression region, pressure gradually increases. From these observations, a favorable pressure gradient immediately behind the nose is caused by the geometry transformation from the blunt nose to the flaring region. In the flaring region, an adverse pressure gradient is caused by the concave surface. Moreover, the flaring region of the cone is designed such that the boundary-layer thickness over the region is close to constant. Due to this fact, the peak frequency of the second-mode-dominated disturbances does not shift as the flow develops downstream [23].

Figure 1b shows the LST-predicted *N* factors for five sampling frequencies within the second-mode range: 260, 270, 278, 285, and 290 kHz. According to the LST analysis, the most amplified frequency among the five sampling ones is 285 kHz. Therefore, in the current roughness control design, 285 kHz has been picked as the most dangerous frequency, and the roughness control method is designed to damp disturbances in a frequency band around 285 kHz.

III. Roughness Design for Second-Mode Control

The control strategy design is based on the result in work by Fong et al. [18]. The idea is to place 2-D roughness elements downstream of the synchronization location of the most dangerous second-mode disturbance, which is determined by LST to be around 285 kHz. The roughness elements are selected to damp this most unstable disturbance, which can eventually lead to transition. In the design, roughness elements with a height less than the local boundary-layer thickness are used. The shape of each roughness element is a half-ellipse, which can be expressed by the following equation:

$$\frac{(x - x_c)^2}{a^2} + \frac{y^2}{b^2} = h^2$$

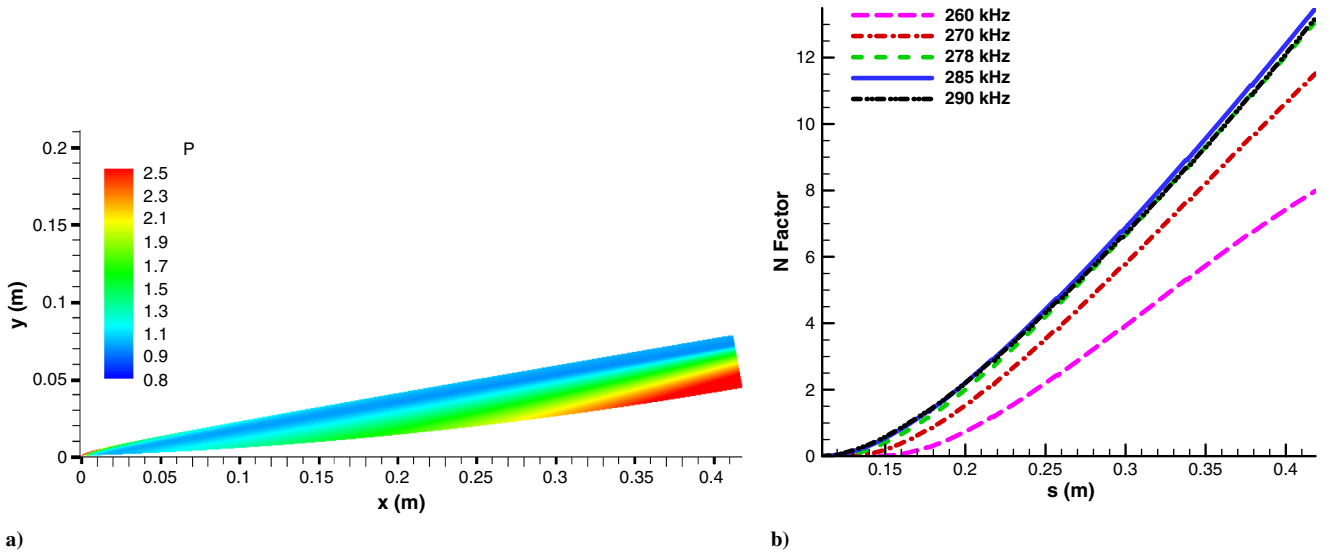

a) b)

Fig. 1 Representations of a) contours of pressure of steady base flow and b) LST-predicted *N* factors.

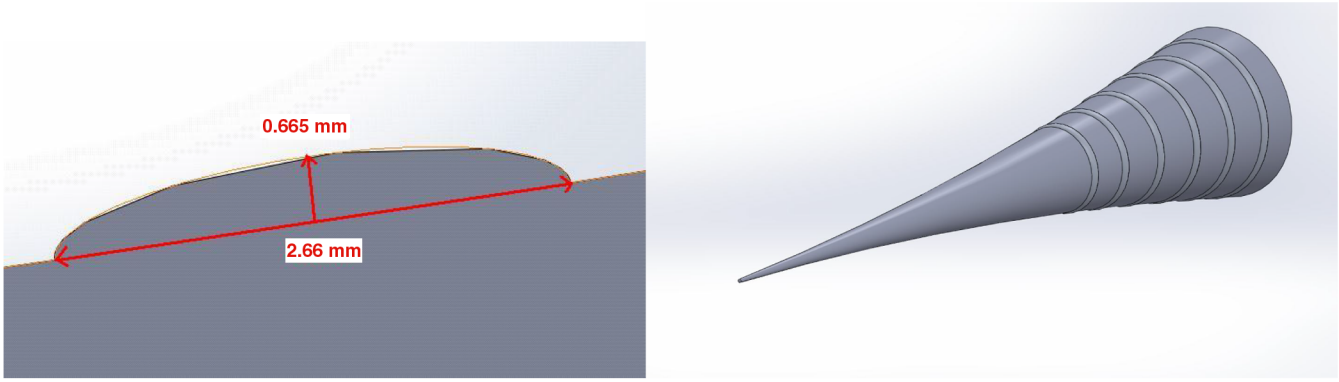

a) b)

Fig. 2 Schematic of the size of the 2-D roughness element.

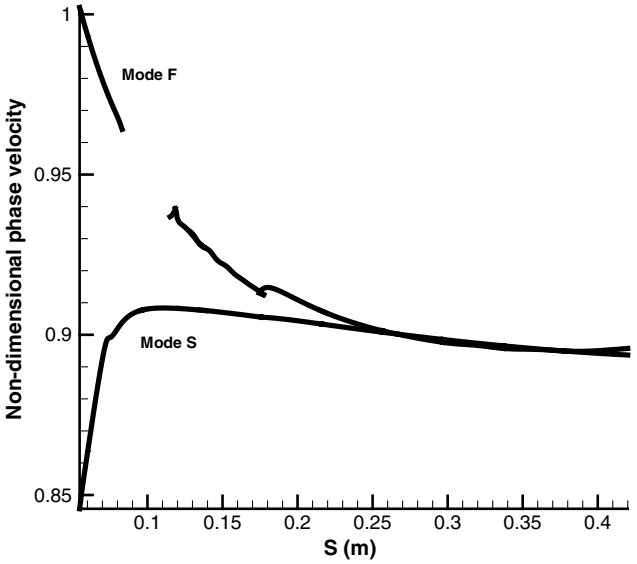

Fig. 3 Phase velocity for 285 kHz disturbance.

where the parameters a, b, and h control the roughness, width, and height. In addition, x_c defines the location of the roughness center. The height and width of a roughness element are defined by the local boundary-layer thickness. The roughness height in the current design is 50% of the local boundary-layer thickness, and the width is two times the local boundary-layer thickness. This particular roughness size is chosen because, in the previous study by Fong et al. [19], this roughness size has shown effective damping effects on the second mode. On the other hand, based on the fact that the local boundary-layer thickness is constant, the size of each roughness element is the same. In the current design, the roughness size is 0.665 mm high and 2.66 mm wide, as shown in Fig. 2a.

As discussed previously, the most dangerous frequency in the current design setup is chosen to be 285 kHz. The phase velocity plot of this frequency is shown in Fig. 3. It can been seen that, for this frequency, the phase velocity of mode F and mode S meet at about 0.25 m along the surface of the cone. This point is the synchronization location of the two modes at this frequency. As a result, in the current design strategy, the first roughness is placed downstream of the synchronization point at $S = 0.3$ m. It has been shown in [18] that roughness elements can damp the second-mode disturbances. However, [18] has also shown that the roughness amplifies the 2-D first mode disturbances in the lower frequencies region. To damp these amplified disturbances at lower frequencies, roughness elements needed to be placed behind the synchronization locations of those amplified disturbances. Since the location of the synchronization point is in inverse proportion to the frequency [18], the synchronization locations for disturbances at frequencies lower than the most dangerous frequency (285 kHz) must be located downstream of the first roughness element. Therefore, multiple roughness elements are to be placed downstream of the first roughness, as shown in Fig. 2b. This multiple roughness design can ensure roughness elements not only damp the most dangerous frequency but also disturbances at the lower-frequency region for which the synchronization locations are behind the first roughness. Another advantage of the design is that it can guarantee that the least-stable second-mode disturbance remains damped downstream. The spacing between adjacent roughness elements is about 10 times their width. The detail location of each roughness elements is shown in Table 1. It should also be noted that Mack [29] has shown the most unstable first mode is three-dimensional (3-D) with an oblique wave angle. It is currently not clear how the 2-D roughness elements will affect the 3-D first mode. Further studies are needed to elucidate this effect.

In the LST calculation of the synchronization location on a smooth surface, the coordinate is based on the surface length S, measured from the nose tip along the cone surface. For convenience of implementation in the experiment, the roughness locations measured from the nose tip along the horizontal direction x have been included in the table. Each roughness element is a ring that is mounted on the surface of the compression cone. Consequently, the roughness effects on the cone are limited to 2-D. Figure 2b shows the 3-D CAD drawing of the roughness design. It can be seen in Fig. 2b that six roughness rings are mounted on the aft end of the cone according to the design in Table 1.

IV. Experimental Results

A. Experimental Setup

Experiments were conducted at the Boeing/AFOSR Mach 6 quiet wind tunnel at Purdue University, where 2-D roughness elements were applied to a flared cone with a 3 m radius of curvature and a 1 mm nose tip. PCB132 fast-pressure sensors were used to measure the frequencies and amplitude of instabilities within the boundary layer. Temperature-sensitive paint was used to measure the global heat transfer on the model [30]. The cone was instrumented as shown in Fig. 4. The main sensor array had eight holes, which are sized for PCB sensors. For the experiment, five were used for PCB sensors and one was used for a Schmidt–Boelter (SB) gauge for calibrating the temperature-sensitive paint. There are also two more rows of sensor holes located 120 deg in both directions from the main array. The "left array" is 120 deg counterclockwise from the main array, as seen by

Table 1 Detailed locations for each roughness element

Roughness number	1	2	3	4	5	6
S (center of roughness), m	0.3	0.3266	0.3532	0.3798	0.4064	0.433
x (center of roughness), m	0.2985	0.3226	0.3503	0.3783	0.4045	0.4298

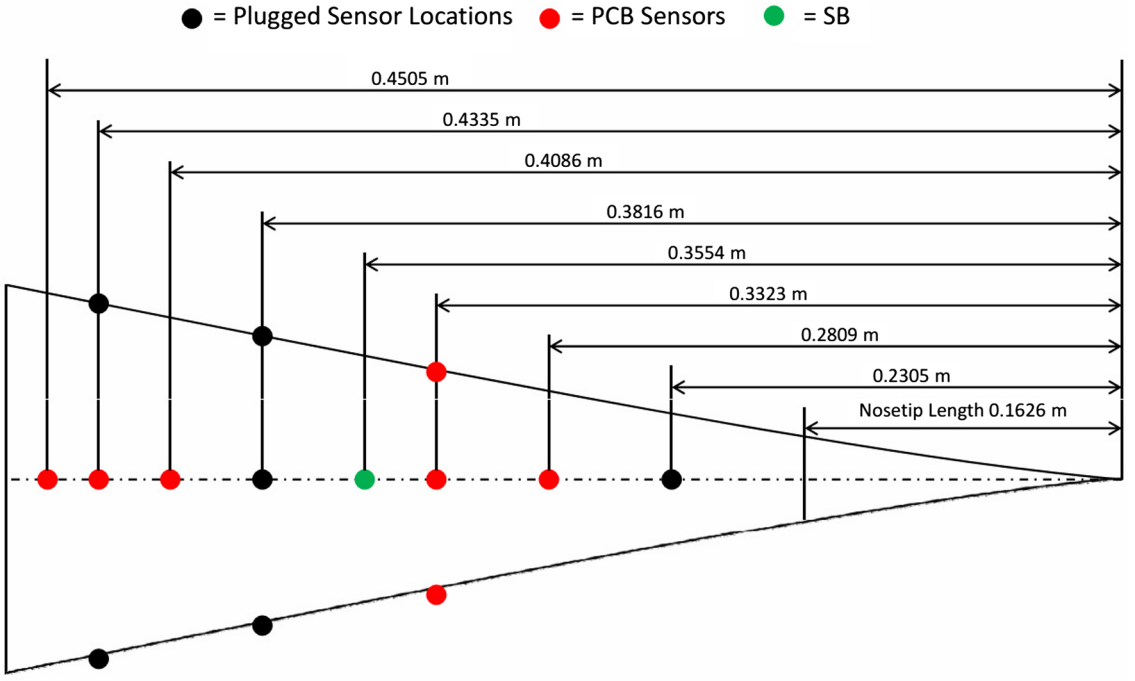

Fig. 4 Experimental setup.

the flow; and the "right array" is 120 deg clockwise. For the experiment, only one sensor was placed on each array. All unused sensor holes were plugged so as not to disrupt the flow.

B. Experiment and Simulation Comparison

In addition to the roughness experiment, simulation results for an unsteady flow over the same cone without roughness obtained by Huang and Zhong [23] are compared with those measured in the case of a smooth cone of the current experiment. It should be pointed out that the unsteady simulation results of [23] are induced by an entropy spot perturbation in the freestream, whereas the second-mode waves in the current experiment are induced by background noise in the wind tunnel. Despite the differences, the second-mode growth of these two sets of results can still be compared as long as the comparison is on the relative growth of the second mode after it undergoes exponential growth in the unstable region. It should also be noted that the excited second-mode instability does not depend on the disturbance source as long as the disturbance is small and in the linear region. For example, the second-mode instability range matches in [7] and [18], although different disturbance sources (blowing and suction, pure mode S/F, and a pulse), are imposed into the same freestream conditions. In the current simulation, disturbances of 0.001% of the corresponding freestream values are used and the experiment is performed in a quiet tunnel. Therefore, the disturbance of the second mode in the current paper is linear and can be separated using a Fourier transform.

The relative amplitudes of the simulation results are normalized by the second-mode peak value of the experimental results at $x = 0.4\ m$. The normalized simulation amplitudes and experimental amplitudes are compared in Fig. 5. Because the comparison is not about the absolute amplitudes, the relative growth of the second mode should be independent of the original source of the perturbations in the linear second-mode dominated regime. Therefore, such a comparison is made here in order show the simulations of the second mode agree with the experiment for the second-mode growth. It serves as verification between the two separate sets of results: numerical and experimental ones.

The comparison of spectra between the unsteady hotspot simulation and the current experiment with freestream noise over a smooth cone is shown in Fig. 5. Noticeably, the experimental result has a stagnation pressure of 150 psia, and the one in the simulation is 140 psia. The experimental result is completed at a stagnation

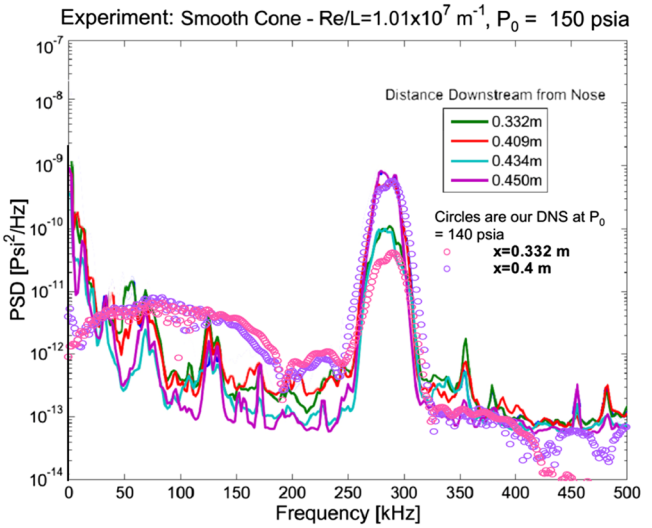

Fig. 5 Comparison of spectra between the hotspot simulation and experiment of the smooth cone. The experimental amplitudes are expressed in power spectral density (PSD).

temperature of 323.2°F, whereas in the simulation, it is 319°F. However, the unit Reynolds number is the same. The experimental results shown in Fig. 5 are given in four locations. For the simulation results, two locations ($x = 0.332$ and 0.4 m) are available for comparison with the experiment.

Overall, Fig. 5 shows a good agreement for the frequency range of the most unstable second mode between the experiment and the simulation. In particular, the most unstable second-mode frequency range is from 252 to 320 kHz for the experiment, as compared to the range from 246 to 325 kHz for the simulation. Moreover, the experimental most amplified frequency is 280 kHz, compared to 285 kHz in the simulation. The agreement is reasonably good. In addition, the comparison of the overall relative amplitudes in this second-mode region is reasonably well, with the exception of the amplitudes near the peak frequency. Specifically, the relative amplitude of the peak obtained by the simulation at $x = 0.332\ m$ is lower than the experiment. The reason for the difference is still unknown.

C. Experimental Result on Designed Roughness

In the roughness control design, the desired locations and geometries of the roughness strips were calculated by the UCLA group, and they are shown in Table 1. Roughness strips were applied using two layers of high-temperature tape. Each layer of the tape was roughly 0.33 mm thick, although variations of 0.002 mm were measured between new tape and tape that had been applied the day before. This resulted in a roughness height of 0.66 mm, which was slightly lower than the desired height of 0.665 mm. The locations of the roughness strips were outlined using a marker that was placed in a mill. The three-axis location readout of the mill was used to accurately find the upstream edge of each roughness strip. The cone was then slowly rotated 360 deg so the marker would draw a line for the beginning of the roughness strip. Roughness strips 4 and 5 would have covered a PCB sensor if they were placed in their desired locations. Both strip locations were consequently moved upstream by 1.33 mm. The desired width of the roughness strips was 2.66 mm. To ensure this, a digital caliper was set to 2.66 mm, locked into place, and used to make small indentations in the tape. Those indentations were used as guidelines to cut the tape using a tabletop paper trimmer.

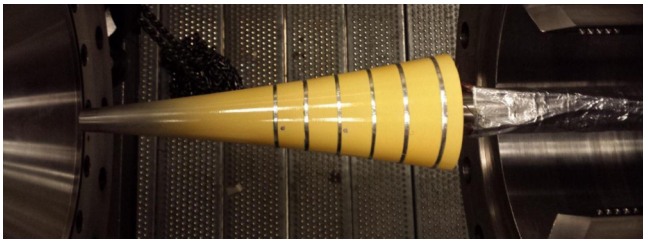

Fig. 6 Photograph of the compression cone with roughness design.

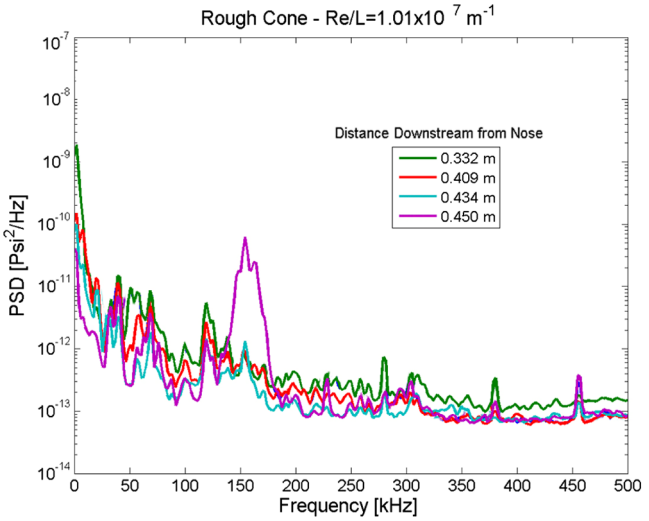

Fig. 7 Power spectral density along flared cone with roughness elements.

Once cut, the strips were placed on the model by hand and smoothed out. Figure 6 shows a photograph of the model with all of the roughness strips applied.

In the previous section, Fig. 5 shows the experimental power spectral density on the flared cone without roughness with freestream noise. The second-mode peak can be clearly seen around 285 kHz. The same power spectra for the case with applied roughness design can be seen in Fig. 7. Comparing with Fig. 5, Fig. 7 shows that the second-mode peaks near 285 kHz are no longer the major disturbance and are concealed by the noise floor of the sensors. Another peak is located around 150–155 kHz. This concurs with the idea that the roughness behind a certain frequency's synchronization point damps the target frequency and amplifies lower frequencies. For comparison, the wave amplitude is nondimensionalized by the calculated mean pressure over the smooth cone ($P'_{\mathrm{rms}}/P_{\mathrm{mean}}$). For the 150 kHz peak on the rough cone, it is 0.0030, whereas the second-mode peak at 285 kHz for the smooth case has an amplitude of 0.0164. The ratio of the 285 kHz peak to the 150 kHz peak is 5.47. Overall, the amplified disturbances at lower frequencies are still an order of magnitude lower than the second mode on a smooth cone.

Figure 8 shows the temperature-sensitive paint images for the smooth and rough cases. In Fig. 8a (the smooth case), we start to see heating associated with the saturation and breakdown of the second-mode waves, at the very base of the cone. For Fig. 8b (the rough case), this heating is not present. Also note that the roughness elements do not generate significant secondary local heating on the cone. On the cone with the roughness design, the boundary layer seems less unstable and the second-mode breakdown is not present.

V. Conclusions

In this Note, the design of a set of 2-D roughness elements for the second-mode control on a flared cone is presented, along with the corresponding experimental results. Experiments were conducted at Purdue University on a flared cone with a 3 m radius of curvature and strips of roughness applied at specific locations. The testing was based on the calculations performed at UCLA.

The comparison involving the most amplified second-mode disturbance between the simulation and experiment for the smooth cone shows a reasonably good agreement. Both the numerical simulation and experiment show the second-mode peak is around 285 kHz. For the experimental test of the cone with designed roughness elements, PCB132 pressure data show the second-mode instability to be completely damped on the rough cone, whereas possible first-mode instability at 150 kHz is possibly amplified. The amplitudes of the dominant peaks in the frequency spectrum measured on the cone were reduced by a factor of five. Global heat transfer measurements qualitatively confirm the result by showing reduction of global transitional heating on the model. Overall, the experiment shows that the idea of using 2-D roughness elements to damp second-mode waves can work, i.e., judiciously placed roughness elements downstream of the synchronization point can damp the most amplified disturbances.

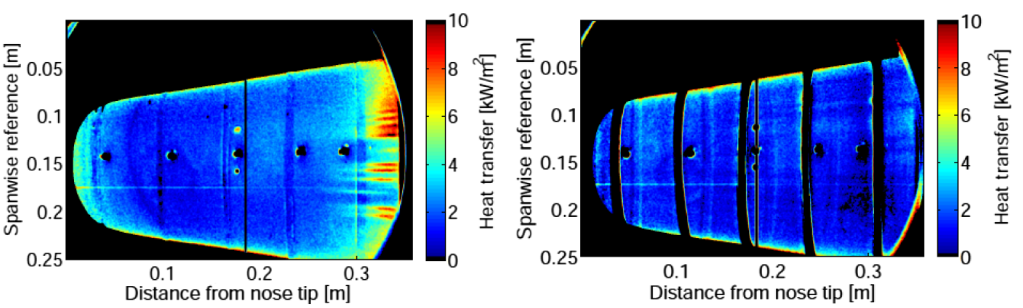

Fig. 8 Temperature-sensitive paint images for the smooth and rough cases.

Acknowledgments

This work was sponsored by the U.S. Air Force Office of Scientific Research (AFOSR), the U.S. Air Force, under AFOSR grants FA9550-07-1-0414 and FA9550-12-1-0167, monitored by John Schmisseur and Rengasamy Ponnappan. This work was also sponsored by the AFOSR/NASA National Center for Hypersonic Research in Laminar-Turbulent Transition. The views and conclusions contained herein are those of the author and should not be interpreted as necessarily representing the official policies or endorsements either expressed or implied, of the U.S. Air Force Office of Scientific Research or the U.S. Government.

References

[1] Schneider, S. P., "Summary of Hypersonic Boundary-Layer Transition Experiments on Blunt Bodies with Roughness," *Journal of Spacecraft and Rockets*, Vol. 45, No. 6, 2008, pp. 1090–1105. doi:10.2514/1.37431

[2] Saric, W. S., Reed, H. L., and Kerschen, E. J., "Boundary-Layer Receptivity to Freestream Disturbances," *Annual Review of Fluid Mechanics*, Vol. 34, Jan. 2002, pp. 291–319. doi:10.1146/annurev.fluid.34.082701.161921

[3] James, C. S., "Boundary Layer Transition on Hollow Cylinders in Supersonic Free Flight as Affected by Mach Number and a Screwthread Type of Surface Roughness," NASA TR-Memo-1-20-59A, 1959.

[4] Holloway, P. F., and Sterrett, J. R., "*Effect of Controlled Surface Roughness on Boundary-Layer Transition and Heat Transfer at Mach Numbers of 4.8 and 6.0*," NASA TN-D-2054, 1964.

[5] Fujii, K., "Experiment of the Two-Dimensional Roughness Effect on Hypersonic Boundary-Layer Transition," *Journal of Spacecraft and Rockets*, Vol. 43, No. 4, 2006, pp. 731–738. doi:10.2514/1.17860

[6] Marxen, O., Iaccarino, G., and Shaqfeh, E. S. G., "Disturbance Evolution in a Mach 4.8 Boundary Layer with Two-Dimensional Roughness-Induced Separation and Shock," *Journal of Fluid Mechanics*, Vol. 648, April 2010, pp. 435–469. doi:10.1017/S0022112009992758

[7] Duan, L., Wang, X., and Zhong, X., "A High-Order Cut-Cell Method for Numerical Simulation of Hypersonic Boundary-Layer Instability with Surface Roughness," *Journal of Computational Physics*, Vol. 229, No. 19, 2010, pp. 7207–7237. doi:10.1016/j.jcp.2010.06.008

[8] Riley, Z. B., McNamara, J. J., and Johnson, H. B., "Hypersonic Boundary Layer Stability in the Presence of Thermo-Mechanical Surface Compliance," AIAA Paper 2012-1549, 2012.

[9] Riley, Z. B., McNamara, J. J., and Johnson, H. B., "Assessing Hypersonic Boundary-Layer Stability in the Presence of Structural Deformation," *AIAA Journal*, Vol. 52, No. 11, 2014, pp. 2547–2558. doi:10.2514/1.J052941

[10] Egorov, I. V., Novikov, A.V., and Fedorov, A. V., "Direct Numerical Simulation of Supersonic Boundary Layer Stabilization Using Grooved Wavy Surface," AIAA Paper 2010-1245, 2010.

[11] Balakumar, P., "Stability of Hypersonic Boundary-Layers over a Compression Corner," AIAA Paper 2002-2848, 2002.

[12] Egorov, I. V., Fedorov, A. V., and Novikov, A.V., "Numerical Modeling of the Disturbances of the Separated Flow in a Rounded Compression Corner," *Fluid Dynamics*, Vol. 41, No. 4, 2006, pp. 521–530. doi:10.1007/s10697-006-0070-7

[13] Bountin, D., Chimitov, T., Maslov, A., Novikov, A., Egorov, I., Fedorov, A., and Utyuzhnikov, S., "Stabilization of Hypersonic Boundary Layer Using a Wavy Surface," *AIAA Journal*, Vol. 51, No. 5, 2013, pp. 1203–1210. doi:10.2514/1.J052044

[14] Duan, L., Wang, X., and Zhong, X., "A High-Order Cut-Cell Method for Numerical Simulation of Hypersonic-Boundary Transition with Arbitrary Surface Roughness," AIAA Paper 2009-1337, 2009.

[15] Ma, Y., and Zhong, X., "Receptivity of a Supersonic Boundary Layer over a Flat Plate. Part 1: Wave Structures and Interactions," *Journal of Fluid Mechanics*, Vol. 488, July 2003, pp. 31–78. doi:10.1017/S0022112003004786

[16] Ma, Y., and Zhong, X., "Receptivity of a Supersonic Boundary Layer over a Flat Plate. Part 2: Receptivity to Freestream Sound," *Journal of Fluid Mechanics*, Vol. 488, July 2003, pp. 79–121. doi:10.1017/S0022112003004798

[17] Fong, K. D., Wang, X., and Zhong, X., "Finite Roughness Effect on Modal Growth of a Hypersonic Boundary Layer," AIAA Paper 2012-1086, 2012.

[18] Fong, K. D., Wang, X., and Zhong, X., "Numerical Simulation of Roughness Effect on the Stability of a Hypersonic Boundary Layer," *Computers and Fluids*, Vol. 96, June 2014, pp. 350–367. doi:10.1016/j.compfluid.2014.01.009

[19] Fong, K. D., Wang, X., and Zhong, X., "Stabilization of Hypersonic Boundary Layer by 2-D Surface Roughness," AIAA Paper 2013-2985, 2013.

[20] Park, D., and Park, S. O., "Study on Stabilization and Destabilization Effect of a Smooth Hump in Hypersonic Boundary Layer by PSE," AIAA Paper 2013-2742, 2013.

[21] Fong, K. D., Wang, X., and Zhong, X., "Numerical Simulation of Roughness Effect on the Stability of a Hypersonic Boundary Layer," *Seventh International Conference on Computational Fluid Dynamics (ICCFD7)*, Organization Paper 1502, Big Island, HI, July 2012.

[22] Wheaton, B. M., Juliano, T. J., Berridge, D. C., Chou, A., Gilbert, P. L., Casper, K. M., Steen, L. E., and Schneider, S. P., "Instability and Transition Measurements in the Mach-6 Quiet Tunnel," AIAA Paper 2009-3559, 2009.

[23] Huang, Y., and Zhong, X., "Numerical Study of Hypersonic Boundary-Layer Receptivity with Freestream Hotspot Perturbations," *AIAA Journal*, Vol. 52, No. 12, 2014, pp. 2652–2672. doi:10.2514/1.J052657

[24] Chynoweth, B., Ward, C., Greenwood, R., McKiernan, G., Fisher, R., and Schneider, S., "Measuring Transition and Instabilities in a Mach 6 Hypersonic Quiet Wind Tunnel," AIAA Paper 2014-2643, 2014.

[25] Huang, Y., and Zhong, X., "Numerical Study of Laser-Spot Effects on Boundary-Layer Receptivity for Blunt Compression-Cones in Mach-6 Freestream," AIAA Paper 2010-4447, 2010.

[26] Huang, Y., and Zhong, X., "Numerical Study of Freestream Hot-Spot Perturbation on Boundary-Layer Receptivity for Blunt Compression-Cones in Mach-6 Flow," AIAA Paper 2011-3078, 2011.

[27] Huang, Y., and Zhong, X., "Numerical Study of Boundary-Layer Receptivity on Blunt Compression-Cones in Mach-6 Flow with Localized Freestream Hot-Spot Perturbations," *RTO Applied Vehicle Technology Panel (AVT) Specialists' Meeting on Hypersonic Laminar-Turbulent Transition*," NATO Science and Technology Organization Paper 20, San Diego, CA, April 2012.

[28] Huang, Y., and Zhong, X., "Parametric Study of Boundary-Layer Receptivity to Freestream Hot-Spot Perturbation over a Blunt Compression Cone," AIAA Paper 2014-0774, 2014.

[29] Mack, L. M., "Boundary Layer Linear Stability Theory," AGARD Rept. 709, 1984, pp. 1–81.

[30] Sullivan, J. P., Schneider, S. P., Liu, T., Rubal, J., Ward, C., Dussling, J., Rice, C., Foley, R., Cai, Z., Wang, B., and Woodiga, S., "Quantitative Global Heat Transfer in a Mach-6 Quiet Tunnel," NASA TR-NASA/CR-2012-217331, Feb. 2012.

M. Choudhari
Associate Editor